J | P | S | T

http://jpst.irost.ir

Journal of

Particle Science and Technology

IROST

Preparation and application of meso-adsorbent NiFe₂O₄ for the ultrasound-enhanced removal of dye pollutant in water and wastewater: A multivariate study

**Behnaz Sarani¹, Mashaallah Rahmani¹,*, Ahmad Reza Abbasian²**

¹ Department of Chemistry, Faculty of Sciences, University of Sistan and Baluchestan, Zahedan 98135-674, Iran
² Department of Materials Engineering, Faculty of Engineering, University of Sistan and Baluchestan, Zahedan 98135-674, Iran

HIGHLIGHTS

• Herein, we present a new combustion method for the preparation of meso-adsorbent NiFe₂O₄ powders.

• SEM, XRD, and BET analysis were used to characterize absorbency.

• To increase the adsorption efficiency, surface methodology (RSM) and artificial neural network (ANN) methods were used to optimize, model and predict the responses.

GRAPHICAL ABSTRACT
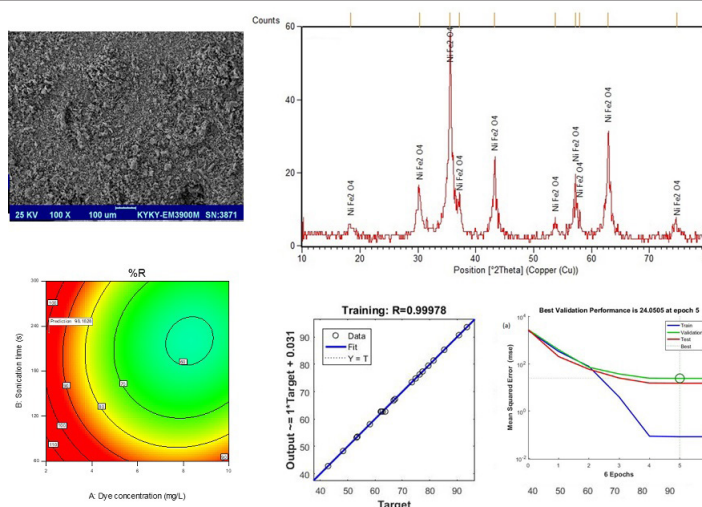
ARTICLE INFO

ABSTRACT

In this study, we present a new combustion method for the preparation of meso-adsorbent NiFe₂O₄ powders. SEM, XRD, and BET were used for the characterization of adsorbents. BET measurements confirmed a specific surface area (SSA) of 87.7 $m^2.g^{-1}$, a total pore volume (PV) of 0.2377 $cm^3.g^{-1}$, and a mean pore size (PS) of 10.841 nm. The mean crystallite diameter of the adsorbent using the Scherrer equation was 10 nm. Also, the response surface methodology and artificial neural network models were used for modeling, optimization, and prediction of responses for removing methyl violet from water and wastewater in lab-scale batches. To study absorption, a four-factor central composite design was used to select the best experimental condition for ultrasonic-assisted adsorption of methyl violet dye. The adjusted R^2 of 0.9931 and the predicted R^2 of 0.9813 are very close, indicating the compatibility of the experimental results with the quadratic model. According to the results, optimum conditions were set at an ultrasonic time of 231 s, 13.5 mg of adsorbent, a dye concentration of 2.0 $mg.L^{-1}$, and a pH = 7.9. Also, the learning rule of Levenberg–Marquardt was used for ANN Modeling. According to the proposed ANN, the value of the root mean square error (RMSE) was 2.562, and the value of the correlation coefficient (R^2) was 0.986. Also, removal efficiencies of 96.8% and 95.57% were obtained for the tap water and wastewater, respectively.

1. Introduction

Due to their broad application, dyes are released into the environment by many different industries [1]. Most of these industries do not appropriately refine their wastewater [2]. Dyes can enter environmental water and threaten human health [3-5]. Among several methods for removing pollutants from wastewater, adsorption seems to be the simplest technique for the effective removal of toxic pollutants in water and wastewater [6-10].

Developing a highly efficient adsorbent with enhanced removal efficiency for dye pollutants is urgently needed. Researchers have recently become interested in the use of nanoparticles to remove contaminants [11-13]. Many nanoparticles and methods have been reported for removing dyes, and the factors affecting removal efficiency, such as dye concentration, adsorbent dosage, pH, and contact time, were studied and optimized. Mall *et al.* [14] utilized bagasse fly ash to remove methyl violet. Musyoka and Mittal also adsorbed methyl violet using functionalized cellulose [15]. Keyhanian *et al.* employed the Fe_3O_4 magnetic nanoparticle to remove methyl violet in aqueous solutions [16]. Tang *et al.* developed effective palygorskite/carbon composites for sustainable, efficient removal of methyl violet [17]. Studies conducted by Jiang *et al.* reported that activated carbon/$NiFe_2O_4$ was used for the adsorption of methyl orange [18]. In other studies, $NiFe_2O_4$/activated carbon [19] and $NiFe_2O_4$/chitosan [20] were used to remove Direct Red 31 and Cd (II) Ion in aqueous solutions, respectively.

In this study, our research group presents a new combustion method for preparing a meso-adsorbent $NiFe_2O_4$ and its application for effective removal of methyl violet (MV) in water and wastewater using an easy to operate ultrasonic-assisted adsorption (UAA) method. Since univariate processes are time-consuming, labor-intensive, and expensive, multivariate statistic methods are usually a suitable alternative to univariate procedures when several parameters need to be optimized [21]. The significant advantages of multivariate statistic methods, artificial neural network (ANN), and response surface methodology (RSM) models are that they decrease the number of experiments, and consequently, save time, energy, and chemicals. Two powerful statistical methods, ANN and RSM, are widely used for modeling and optimization processing approaches in various fields [22-32]. ANN and RSM were applied in this study to increase the adsorption efficiency and to model, optimize, and predict the factors affecting the proposed method. The significant benefits of ANN and RSM are that they decrease the number of experiments, and consequently, save time, energy, and chemicals. Another benefit is the parallel testing and evaluation of variable effects.

2. Experimental

2.1. Adsorbent preparation

Combustion reactions are a promising technique for the preparation of nanomaterials [33]. Therefore, meso-adsorbent $NiFe_2O_4$ was synthesized using glycine as fuel, $Ni(NO_3)_2.6H_2O$ and $Fe(NO_3)_3.9H_2O$ as precursors, and KCl as an additive (the ratios were 4.44:1:2:2, respectively). The mixture was allowed to boil at 200°C. Moments after the liquid evaporated, a combustion reaction was performed. Finally, the combustion powders were filtered, washed, and dried.

2.2. Apparatus

The analysis of MV was performed with a UV-Vis spectrophotometer (2120 UV plus, Optizen). SEM (EM3900M, KyKy), XRD (Advance D8, Bruker), and BET (Nova 2000, Quantachrome) were used to characterize the adsorbent.

2.3. Procedure

For adsorption studies, a 10 mL aliquot of sample solution (pH = 7.9) containing MV dye (2 mg.L^{-1}) was placed in a centrifuge tube, and 13.5 mg of adsorbent was added to it. Then, the mixture was vigorously shaken using an ultrasonic agitator for 4 min. Finally, the residual dye was separated and analyzed by a UV-Vis spectrophotometer. The removal percentage of MV was calculated as Eq. (1).

$$Removal\ \% = (C_0 - C_e) \times 100/C_0 \tag{1}$$

where C_e and C_0 are the equilibrium and initial MV concentration (mg.L^{-1}), respectively.

2.4. Experimental Design

2.4.1. RSM

For RSM, the Design-Expert version 10 statistical software was used. RSM is an appropriate method to optimize conditions for a particular response that is affected by several factors at the same time [34].

A multivariate design of experiments (DoE) was employed to optimize the responses for the ultrasound-enhanced removal of toxic dye using meso-adsorbent $NiFe_2O_4$ and UAA. Design-Expert version 10 statistical software was used for RSM modeling of the UAA of MV. Then, a four-factor central composite design (CCD) was used to select the best experimental condition for UAA of MV. The input variables consisted of *A*: concentration of dye, *B*: ultrasonic time, *C*: the mass of adsorbent, and *D*: pH. The factors, CCD matrix, and the results observed for each experiment are shown in Table 1. Pre-experimental runs were used to select the actor levels.

2.4.2. ANN

MATLAB R2016b mathematical software was used for the ANN modeling of UAA of MV. Experimental data obtained from RSM was used for ANN modeling. The inputs for the ANN modeling include *A*: concentration of dye, *B*: ultrasonic time, *C*: the mass of adsorbent, and *D*: pH (Table 1). The learning rule of Levenberg–Marquardt was used for the ANN modeling. A series of topologies was applied, in which the number of neurons varied from 2 to 20. For training, validation, and testing, 70, 15, and 15% of data were used, respectively.

3. Results and discussion

3.1. Adsorbent characterization

SEM, XRD, and BET were used to characterize the adsorbent. The BET measurements confirmed the specific surface area of 87.7 $m^2.g^{-1}$, total pore volume of 0.2377 $cm^3.g^{-1}$, and the mean pore size of 10.841 nm. The mean crystallite diameter of the adsorbent from the Scherrer equation was 10 nm. The XRD patterns and the SEM images are shown in Figs. 1 and 2, respectively.

Based on the Joint Committee on Powder Diffraction Standards (JCPDS), the XRD pattern matches JCPDS card no. 044-1485, which denotes the cubic spinel structure of $NiFe_2O_4$. As shown in Fig. 1, miller indexes were added in the XRD pattern of $NiFe_2O_4$. As seen in Fig. 2, the morphology of the $NiFe_2O_4$ powders appears in the form of porous agglomerates consisting of uniform sphere-like shape particles.

3.2. RSM modeling

Table S1 (supplementary file) showed the adequacy of the model testing, which confirmed the second-

Table 1. CCD matrix of factors, the observed result, and predicted results using RSM and ANN.

Run	A	B	C	D	Measured	RSM Predicted	ANN Predicted
1	8	240	10	4	45.5	45.17	49.37
2	6	180	15	6	62.1	62.79	62.73
3	4	120	20	4	74.83	73.73	74.83
4	6	180	15	6	62.81	62.79	62.73
5	6	180	25	6	74.88	77.36	67.38
6	6	180	5	6	40.89	39.12	37.51
7	10	180	15	6	76.3	76.56	76.30
8	6	180	15	2	40.89	41.44	38.20
9	8	120	10	8	59.3	59.95	61.43
10	6	180	15	6	63.75	62.79	62.73
11	8	120	20	8	85.3	83.97	85.30
12	4	240	20	4	58.1	57.55	58.10
13	6	180	15	6	63.67	62.79	62.73
14	2	180	15	6	81.4	81.85	81.40
15	8	240	20	8	66.8	66.78	66.80
16	6	180	15	6	62.29	62.79	62.73
17	8	240	10	8	53.56	53.82	53.55
18	6	180	15	6	62.17	62.79	62.73
19	4	240	10	8	77.36	78.21	77.36
20	6	60	15	6	89.04	89.28	96.46
21	4	120	10	4	48.33	48.45	48.33
22	4	240	20	8	79.5	77.76	79.50
23	8	120	20	4	93.57	92.82	93.57
24	6	300	15	6	66.5	66.97	59.88
25	4	120	20	8	90.67	91.10	90.67
26	4	240	10	4	42.83	43.33	42.83
27	6	180	15	10	67.3	67.46	67.3
28	8	120	10	4	53.25	54.15	53.25
29	8	240	20	4	73.44	72.78	73.44
30	4	120	10	8	80.66	80.48	81.50
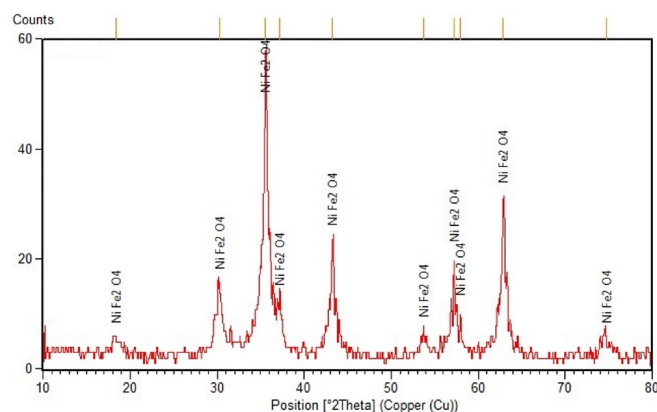
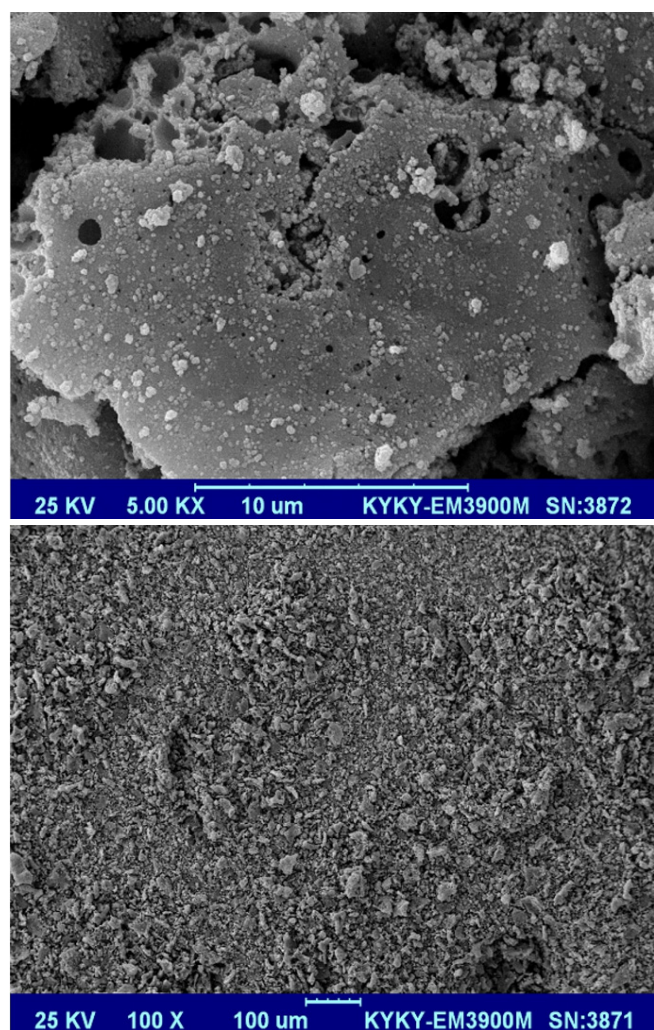**Fig. 1.** XRD patterns of meso-adsorbent NiFe$_2$O$_4$.

Fig. 2. SEM images of meso-adsorbent NiFe$_2$O$_4$.

order model is a good fit for UAA of MV using meso-adsorbent NiFe$_2$O$_4$ powders. The analysis of variance (ANOVA) results are shown in Table 2. The P-value is usually compared against an alpha value of 0.05. If the P-value of a factor is higher than 0.05, the effect of a factor is insignificant in the process. Therefore, a P-value greater than 0.1000 implies that the factor

is insignificant. On the other hand, the F-value of 297.76 means the model is significant. High F-ratio, low p-value, and non-significant lack of fit (P-value = 0.0865) demonstrate that the model is accurate. Also, correlation coefficients, predicted *R*-squared, and adjusted *R*-squared were calculated for the model. Table S1, Table 2, and Fig. S1 (supplementary file) confirm the model compatibility for UAA of MV using meso-adsorbent NiFe$_2$O$_4$ powders. The model coefficients were obtained using Design-Expert version 10 software. The quadratic model can be expressed as Eq. (2).

$$Y\,(Removal\,\%) = -11.29292 - 6.71229 \times A - 0.32542 \times B + 5.12692 \times C + 23.77437 \times D - 8.03125E\text{-}003 \times A \times B + 0.33488 \times A \times C - 1.63906 \times A \times D - 9.21667E\text{-}003 \times B \times C + 5.93750E\text{-}003 \times B \times D - 0.36650 \times C \times D + 1.02563 \times A^2 + 1.06458E\text{-}003 \times B^2 - 0.045550 \times C^2 - 0.52156 \times D^2 \quad (2)$$

3.3. The effects of the parameters

The factors affecting the removal efficiency of dye by meso-adsorbent NiFe$_2$O$_4$ were investigated and

Table 2. ANOVA for response surface model.

Source	SS	DF	MS	F-value	P-value	
Model	6343.10	14	453.08	297.76	< 0.0001	significant
A	42.03	1	42.03	27.62	< 0.0001	
B	747.05	1	747.05	490.96	< 0.0001	
C	2192.68	1	2192.68	1441.04	< 0.0001	
D	1015.56	1	1015.56	667.43	< 0.0001	
AB	14.86	1	14.86	9.77	0.0070	
AC	179.43	1	179.43	117.92	< 0.0001	
AD	687.75	1	687.75	451.99	< 0.0001	
BC	122.32	1	122.32	80.39	< 0.0001	
BD	8.12	1	8.12	5.34	0.0355	
CD	214.92	1	214.92	141.24	< 0.0001	
A²	461.64	1	461.64	303.39	< 0.0001	
B²	402.87	1	402.87	264.77	< 0.0001	
C²	35.57	1	35.57	23.38	0.0002	
D²	119.38	1	119.38	78.46	< 0.0001	
Residual	22.82	15	1.52			
Lack of Fit	20.02	10	2.00	3.57	0.0865	not significant
Pure Error	2.81	5	0.56			
Cor Total	6365.92	29				

optimized. The counterplots for *A*: concentration of dye, *B*: ultrasonic time, *C*: the mass of adsorbent, and *D*: pH are shown in Fig. 3. The pH can also potentially influence the removal efficiency of dyes due to its effect on site dissociation of the adsorbent and hydrolysis of analytes [35]. This factor was investigated from a pH = 2 to 10. Based on the RSM data, the maximum efficiency for removing methyl violet was obtained at pH = 7.9. This could be explained by considering that the surface of the meso-adsorbent $NiFe_2O_4$ was negatively charged, and thus, has a higher tendency for adsorption of MV. Usually, as the contact time increases, the removal efficiency also increases and reaches equilibrium [36].
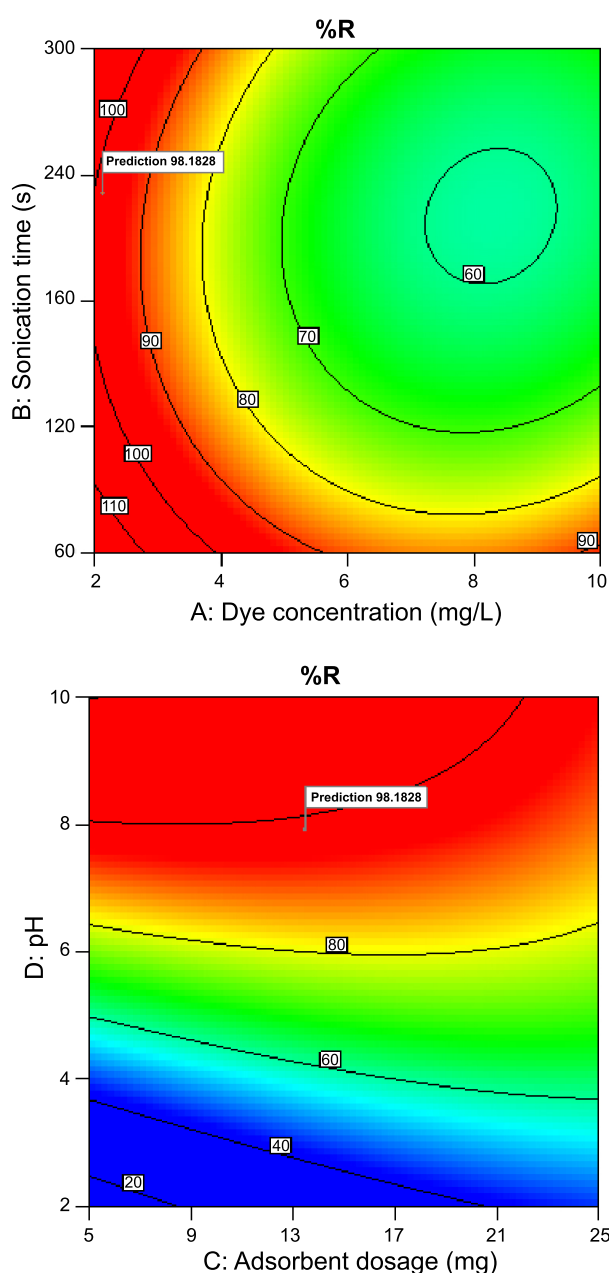
Fig. 3. The counterplots for *A*: concentration of dye, *B*: ultrasonic time, *C*: mass of adsorbent, and *D*: pH.

Therefore, the ultrasonic time can potentially influence the removal efficiency of the analyte due to the effect on the mass transfer of the analyte. In this study, the ultrasonic time was investigated from 1 to 5 minutes (300 s). Results showed that the adsorption efficiency of MV was enhanced with increasing ultrasonic time until 231 s (after equilibrium time), where the removal efficiency stopped showing much improvement or remained constant. This could be attributed to the high surface contact between $NiFe_2O_4$ and MV that enhanced the mass transfer and removal of MV. Based on these results, the best dye concentration was found to be 2.0 mg.L^{-1}. Increasing the concentration of dye in the proposed UAA method decreased the adsorption efficiency due to the saturation of adsorption sites on the adsorbent. In this study, the maximum efficiency for removing methyl violet was obtained at 13.5 mg of $NiFe_2O_4$. When the amount of $NiFe_2O_4$ increased, the adsorption of methyl violet also increased because of improvements in the available adsorption surface sites. According to the RSM data, optimum conditions were set at a dye concentration of 2.0 mg.L^{-1}, ultrasonic time of 231 s (~ 4 min), 13.5 mg of adsorbent, and a pH=7.9 of the sample solution with Desirability=1.

To validate the process, trials were carried out under the optimal conditions to verify optimization results. Table S3 (supplementary file) shows the optimal conditions and model validation for the proposed method. The experimental tests were repeated three times (n=3), and their average values were considered to verify the predicted/optimum value of responses to maximize the ultrasound-enhanced removal of dye pollutants. According to the results (Table S3), the predicted values are very close to the experimental results, having an acceptable validation error of 0.68%.

Table S4 (supplementary file) shows the results obtained from the verification experimental and the calculated value of the proposed method. As observed in Table S4, the error rate ranged between 0.50 and 1.49% for the proposed method. Therefore, the proposed method indicates the relationship between the output and independent input variables well.

3.4. ANN Modeling

The learning rule of Levenberg–Marquardt was used for ANN Modeling. A series of topologies was applied in which the number of neurons varied from 2 to 20.

According to results, the proper network topology of the proposed ANN was found to be 4-9-1, where 4 represents the input layers (concentration of dye, ultrasonic time, the dose of adsorbent, and pH) according to the output layer (removal% of dye) and 9 as hidden neurons. The training parameters of the proposed ANN for the neural network with an optimal number of hidden neurons for UAA of MV were found in Table S2. The regression plots in Fig. S2 (supplementary file) show a comparison between the experimental and the estimated values using the ANN (training, validation, and testing) model for the ultrasound-enhanced removal of dye pollutant by meso-adsorbent $NiFe_2O_4$. According to the proposed ANN, the root mean square error (RMSE) was 2.562, and the correlation coefficient (R^2) was 0.986. Fig. 4(a) shows the mean squared error (MSE) vs the number of epochs for the proposed ANN. As seen in the figure, the training stopped (best validation performance) after epoch numbers 5 for the ultrasound-enhanced adsorption of dye pollutant by meso-adsorbent $NiFe_2O_4$. Also, Fig. 4(b) shows the Error Histogram for the optimal ANN model. This image indicates that the errors are low for the ultrasound-enhanced adsorption of dye by meso-adsorbent $NiFe_2O_4$.

3.5. Analysis of real samples

To study the applicability of the proposed method, an analysis of real samples was investigated. First, tap water and wastewater were filtered, and then the proposed UAA was performed on them. Then, to study the effect of the matrix on dye analysis, the recovery was carried out by spiking the samples with the analyte. Excellent removal efficiencies of 96.8 and 95.57% were obtained for tap water and wastewater, respectively.

Table 3 showed a comparison between other previously reported dates and the proposed method. As seen, the contact time for obtaining the higher removal percentage in the proposed method is less than in other methods. The ultrasound-enhanced removal of dye pollutant could be attributed to high-pressure shock waves during the violent collapse of cavitation bubbles that occurs during the proposed process.

4. Conclusion

In summary, we first presented a new combustion method for preparing meso-adsorbent $NiFe_2O_4$ to
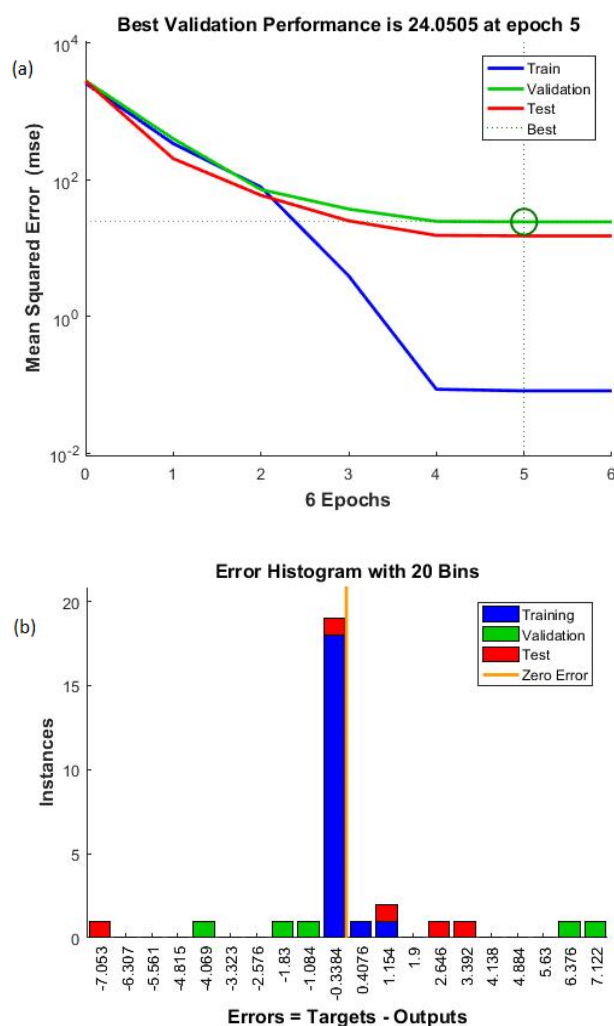
Fig. 4. (a) The mean squared error (MSE) vs. the number of epochs and (b) Error Histogram for the ultrasound-enhanced removal of dye pollutant by meso-adsorbent $NiFe_2O_4$.

develop a combination of ultrasonic with $NiFe_2O_4$ nanomaterial to produce a fast, efficient, and easy-to-use adsorption method for the removal of methyl violet pollutants from water and wastewater in lab-scale batches. The BET measurements confirmed the specific surface area of 87.7 $m^2.g^{-1}$, total pore volume of 0.2377 $cm^3.g^{-1}$, and mean pore size of 10.841 nm of the adsorbent. The mean crystallite diameter of the adsorbent calculated with the Scherrer equation was 10 nm. According to the RSM model, the adjusted R^2 of 0.9931 and the predicted R^2 of 0.9813 are very close, indicating the compatibility of the experimental results with the quadratic model. According to the proposed ANN, the root mean square error was 2.562, the correlation coefficient was 0.986, and the errors were low. It was observed that the combination of ultrasonic with $NiFe_2O_4$ nanomaterial is a fast, efficient, and easy-to-use adsorption method for the removal of

Table 3. Optimal conditions of some of the other previously reported dates and the proposed method.

Adsorbent	Analyte	pH	Adsorbent dosage (g)	Initial dye concentration (mg.L^{-1})	Contact time (min)	Ref.
BFA[a]	Methyl violet	9	0.2	5	120	[14]
FC[b]	Methyl violet	7	0.1	50	45	[15]
Fe_3O_4 MNP[c]	Methyl violet	3	0.01	5	10	[16]
Pal/C[d]	Methyl violet	10	0.02	200	120	[17]
AC/NiFe$_2$O$_4$	Methyl orange	3	0.3	100	30	[18]
NiFe$_2$O$_4$/AC[f]	Direct red 31	2	0.02	20	20	[19]
NiFe$_2$O$_4$-CS[g]	Cd (II)	7	0.2	10	60	[20]
NiFe$_2$O$_4$ meso-adsorbent	Methyl violet	7.9	0.01	2	4	This study

[a]Bagasse fly ash, [b]Functionalized cellulose, [c]Fe_3O_4 Magnetic nanoparticle, [d]Palygorskite/Carbon composite, [e]Activated carbon/NiFe$_2$O$_4$, [f]NiFe$_2$O$_4$/Activated carbon, [g]NiFe$_2$O$_4$-Chitosan.

methyl violet pollutants from water and wastewater. According to our results, the optimum conditions were set at an ultrasonic time of 231 s, 13.5 mg of adsorbent, dye concentration of 2.0 mg.L^{-1}, and pH=7.9. We can conclude that the obtained good adsorption efficiencies indicate that the ultrasound-enhanced adsorption by meso-adsorbent NiFe$_2$O$_4$ shows good potential for the removal of toxic dyes from water and wastewater.

Acknowledgment

Conflict of interest

The authors declare that they have no conflict of interest.

References

[1] L. Liu, Z.Y. Gao, X.P. Su, X. Chen, L. Jiang, J.M. Yao, Adsorption removal of dyes from single and binary solutions using a cellulose-based bioadsorbent, ACS Sustain. Chem. Eng. 3 (2015) 432-442.

[2] T. Robinson, G. McMullan, R. Marchant, P. Nigam, Remediation of dyes in textile effluent: a critical review on current treatment technologies with a proposed alternative, Bioresource Technol. 77 (2001) 247-255.

[3] K. Sinha, P.D. Saha, S. Datta, Extraction of natural dye from petals of Flame of forest (Butea monosperma) flower: Process optimization using response surface methodology (RSM), Dyes Pigments, 94 (2012) 212-216.

[4] V.K. Gupta, G. Sharma, D. Pathania, N.C. Kothiyal, Nanocomposite pectin Zr (IV) selenotungsto-phosphate for adsorptional/photocatalytic remediation of methylene blue and malachite green dyes from aqueous system, J. Ind. Eng. Chem. 21 (2015) 957-964.

[5] A. Rakhshani Aval, M. Rahmani, E. Ghasemi, Development and optimization of chemometric assisted micro-cloud point extraction for preconcentration and separation of Eriochrome black T in water and wastewater samples, Desalin. Water Treat. 120 (2018) 173-179.

[6] J.L. Gong, B. Wang, G.M. Zeng, C.P. Yang, C.G. Niu, Q.Y. Niu, Y. Liang, Removal of cationic dyes from aqueous solution using magnetic multi-wall carbon nanotube nanocomposite as adsorbent, J. Hazard. Mater. 164 (2009) 1517-1522.

[7] I.N. Savina, C.J. English, R.L. Whitby, Y. Zheng, A. Leistner, S.V. Mikhalovsky, High efficiency removal of dissolved As (III) using iron nanoparticle-embedded macroporous polymer composites, J. Hazard. Mater. 192 (2011) 1002-1008.

[8] S. Hasani, F.D. Ardejani, M.E. Olya, Equilibrium and kinetic studies of azo dye (Basic Red 18) adsorption onto montmorillonite: Numerical simulation and laboratory experiments, Korean J. Chem. Eng. 34 (2017) 2265-2274.

[9] G. Bayramoglu, M.Y. Arica, Adsorption of Congo Red dye by native amine and carboxyl modified biomass of Funalia trogii: isotherms, kinetics and thermodynamics mechanisms, Korean J. Chem. Eng.

35 (2018) 1303-1311.

[10] Z. Jiahua, W. Suying, G. Hongbo, One-pot synthesis of mgnetic graphene nanocomposites decorated with core@double-shell nanoparticles for fast chromium removal, Environ. Sci. Technol. 46 (2012) 977-985.

[11] R. Kaur, A. Hasan, N. Iqbal, S. Alam, M.K. Saini, S.K. Raza, Synthesis and surface engineering of magnetic nanoparticles for environmental cleanup and pesticide residue analysis: A review, J. Sep. Sci. 37 (2014) 1805-1825.

[12] N.N. Nassar, N.N. Marei, Vitale G., L.A. Arar, Adsorptive removal of dyes from synthetic and real textile wastewater using magnetic iron oxide nanoparticles: Thermodynamic and mechanistic insights, Can. J. Chem. Eng. 93 (2015) 1965-1974.

[13] N.S. Mishra, A. Kuila, A. Nawaz, S. Pichiah, K.H. Leong, M. Jang, Engineered carbon nanotubes: Review on the role of surface chemistry, mechanistic features, and toxicology in the adsorptive removal of aquatic pollutants, ChemistrySelect, 3 (2018) 1040-1055.

[14] I.D. Mall, V.C. Srivastava, N.K. Agarwal, Removal of Orange-G and Methyl Violet dyes by adsorption onto bagasse fly ash-kinetic study and equilibrium isotherm analyses, Dyes Pigments, 69 (2006) 210-223.

[15] S.M. Musyoka, H. Mittal, S.B. Mishra, J.C. Ngila, Effect of functionalization on the adsorption capacity of cellulose for the removal of methyl violet, Int. J. Biol. Macromol. 65 (2014) 389-397.

[16] F. Keyhanian, S. Shariati, M. Faraji, M. Hesabi, Magnetite nanoparticles with surface modification for removal of methyl violet from aqueous solutions, Arab. J. Chem. 9 (2016) 348-354.

[17] J. Tang, L. Zong, B. Mu, Y. Zhu, A. Wang, Preparation and cyclic utilization assessment of palygorskite/carbon composites for sustainable efficient removal of methyl violet, Appl. Clay Sci. 161 (2018) 317-325.

[18] T. Jiang, Y.D. Liang, Y.J. He, Q. Wang, Activated carbon/$NiFe_2O_4$ magnetic composite: A magnetic adsorbent for the adsorption of methyl orange, J. Environ. Chem. Eng. 3 (2015) 1740-1751.

[19] M.J. Livani, M. Ghorbani, Fabrication of $NiFe_2O_4$ magnetic nanoparticles loaded on activated carbon as novel nanoadsorbent for Direct Red 31 and Direct Blue 78 adsorption, Environ. Technol. 39 (2018) 2977-2993.

[20] A. Homayonfard, M. Miralinaghi, R. Haji Seyed Mohammad Shirazi, E. Moniri, Removal of Cd (II) Ion from aqueous solution using nickel ferrite magnetic nanoparticles cross-linked chitosan, J. Water Wastewater, 31 (2020) 112-127

[21] C. Chatfield, Introduction to Multivariate Analysis, Routledge, 2018.

[22] J. Hernández-Borges, M.A. Rodríguez-Delgado, F.J. Garcia-Montelongo, Optimization of the microwave-assisted saponification and extraction of organic pollutants from marine biota using experimental design and artificial neural networks, Chromatographia, 63 (2006) 155-160.

[23] I.H. Cho, K.D. Zoh, Photocatalytic degradation of azo dye (Reactive Red 120) in TiO_2/UV system: Optimization and modeling using a response surface methodology (RSM) based on the central composite design, Dyes Pigments, 75 (2007) 533-543.

[24] J.P. Coutinho, G.F. Barbero, O.F. Avellán, A. Garcés-Claver, H.T. Godoy, M. Palma, C.G. Barroso, Use of multivariate statistical techniques to optimize the separation of 17 capsinoids by ultra performance liquid chromatography using different columns, Talanta, 134 (2015) 256-263.

[25] N. Khan, T.G. Kazi, M. Tuzen, M. Soylak, A multivariate study of solid phase extraction of beryllium (II) using human hair as adsorbent prior to its spectrophotometric detection, Desalin. Water Treat. 55 (2015) 1088-1095.

[26] K. Vivek, K.V. Subbarao, B. Srivastava, Optimization of postharvest ultrasonic treatment of kiwifruit using RSM, Ultrason. Sonochem. 32 (2016) 328-335.

[27] E. Ahmadloo, S. Azizi, Prediction of thermal conductivity of various nanofluids using artificial neural network, Int. Commun. Heat Mass, 74 (2016) 69-75.

[28] S.A. Hosseini, M. Davodian, A.R. Abbasian, Remediation of phenol and phenolic derivatives by catalytic wet peroxide oxidation over Co-Ni layered double nano hydroxides, J. Taiwan Inst. Chem. E. 75 (2017) 97-104.

[29] M. Rahmani, E. Ghasemi, M. Sasani, Application of response surface methodology for air assisted-dispersive liquid-liquid microextraction of deoxynivalenol in rice samples prior to HPLC-DAD analysis and comparison with solid phase extraction cleanup, Talanta, 165 (2017) 27-32.

[30] V. Vatanpour, A. Karami, M. Sheydaei, Central composite design optimization of Rhodamine B degradation using TiO_2 nanoparticles/UV/PVDF process in continuous submerged membrane photoreactor, Chem. Eng. Process. 116 (2017) 68-75.

[31] P. Davoodi, S.M. Ghoreishi, A. Hedayati, Optimization of supercritical extraction of galegine from *Galega officinalis L.*: Neural network modeling and experimental optimization via response surface methodology, Korean J. Chem. Eng. 34 (2017) 854-865.

[32] X. Zheng, W. Zheng, J. Zhou, X. Gao, Z. Liu, N. Han, J. Yin, Study on the discrimination between Corydalis Rhizoma and its adulterants based on HPLC-DAD-Q-TOF-MS associated with chemometric analysis, J. Chromatogr. B, 1090 (2018) 110-121.

[33] A.R. Abbasian, M. Shafiee Afarani, One-step solution combustion synthesis and characterization of $ZnFe_2O_4$ and $ZnFe_{1.6}O_4$ nanoparticles, Appl. Phys. A, 125 (2019) 721.

[34] M.A. Bezerra, R.E. Santelli, E.P. Oliveira, L.S. Villar, L.A Escaleira, Response surface methodology (RSM) as a tool for optimization in analytical chemistry, Talanta, 76 (2008) 965-977.

[35] F. Diejing, B. Bo, W. Honglun, S. Yourui, Novel fabrication of PAA/PVA/yeast superabsorbent with interpenetrating polymer network for pH-dependent selective adsorption of dyes, J. Polym. Environ. 26 (2018) 567-588.

[36] M. Rahmani, M. Kaykhaii, M. Sasani, Application of Taguchi L16 design method for comparative study of ability of 3A zeolite in removal of Rhodamine B and Malachite green from environmental water samples, Spectrochim. Acta A, 188 (2018) 164-169.